Heliyon 5 (2019) e02149

Contents lists available at ScienceDirect

Heliyon

journal homepage: www.heliyon.com

# Quantum chemical studies and spectroscopic investigations on 2-amino-3-methyl-5-nitropyridine by density functional theory

S. Sivaprakash [a], S. Prakash [b], S. Mohan [c], Sujin P. Jose [a,*]

[a] Department of Computational Physics, School of Physics, Madurai Kamaraj University, Madurai, 625 021, Tamil Nadu, India
[b] Departmentof Physics, VHNSN College, Virudhunagar, 626 001, Tamil Nadu, India
[c] Department of Physics, S.A. Engineering College, Thiruverkadu, Chennai, 600 077, India

ARTICLE INFO

*Keywords:*
Molecular physics
Materials chemistry
Theoretical chemistry

ABSTRACT

Quantum chemical calculations on energy and molecular structure of 2-amino-3-methyl-5-nitropyridine (2A3M5NP) have been attempted by implementing DFT/B3LYP method using 6-311G (d,p), 6-311G++ (d,p) and cc-pVTZ basis sets. The optimized geometry and the vibrational analysis for energetically most stable configuration, are carried out theoretically by using B3LYP/cc-pVTZ basis set. The computed vibrational frequencies were scaled by using scaling factors and compared with the experimental Fourier Transform Infra-Red (FTIR) solid phase spectrum in the region 4000-400 $cm^{-1}$ and FT-Raman spectrum in the region 4000-100 $cm^{-1}$. The complete vibrational assignments, analysis and correlation of fundamental modes of the compound have been carried out using the potential energy distribution (PED). The intramolecular charge transfer, hyperconjugative interaction of the compound is investigated from natural bonding orbital (NBO) analysis. The UV-Visible spectrum of 2A3M5NP was obtained with ethanol as a solvent. The electronic properties such as HOMO (Highest Occupied Molecular Orbital) and LUMO (Lowest Unoccupied Molecular Orbital) energies are determined by B3LYP/cc-pVTZ basis set. The electronic absorption spectrum of the compound was studied from UV-Visible analysis by using time-dependent density functional theory (TD-DFT). The electron density distribution and chemical reactive sites of 2A3M5NP were analyzed from molecular electrostatic potential (MEP) analysis and frontier molecular orbital (FMO) analysis.

## 1. Introduction

Nitrogen based heterocyclic compounds play an important role in biomedical research and drug designing due to their immense potential against tumor cells. Pyridine is the most important nitrogen based heterocyclic ring system incorporated in the structure of many antimicrobial pharmaceuticals. Pyridine nucleus is prevalent in most of the natural products and is extremely important in the chemistry of biological systems. It plays a key role in catalyzing both biological and chemical systems. The wide-ranging biological activities are associated with many pyridines and its derivatives which ensure the importance of the study of this ring system. Pyridine exhibits antiproliferative [1], anti-HIV [2], anti-bacterial [3], anti-malarial [4], anti-fungal [5], anti-oxidant [6] and antitubulin activities [7, 8]. Pyridine forms the nucleus over 7000 existing drugs in pharmaceutical industries [9]. Pyridine derivatives containing multi-functional groups such as streotonigrin, streptonigrone and lavendamycin are reported as anti-cancer drugs and cerivastain is reported as the HMG-CoA enzyme inhibitor [10]. In many enzymes of living organisms, it is the prosthetic pyridine nucleotide (NADP) that is involved in various oxidation-reduction processes. Pyridine congeners are associated with different biological properties like pesticidal, insecticidal and fungicidal [11]. 2-amino-3-cyano pyridine derivatives have been identified as IKK-B-inhibitors along with their importance and utility as intermediates in preparing a variety of heterocyclic compounds [12]. 1H-pyrozolo [3,4-b] pyridines comprise a very interesting class of compounds because of their significant and versatile biological and pharmacological activities, such as antimicrobial, antimalarial, antiviral and antiproliferative [13].

The vibrational spectroscopy like IR and FT-Raman techniques provide the useful information about the identification of biological system at the molecular level. Both these techniques serve as a spectral fingerprint to study the detailed information of the biological system. On the other hand, the Density functional theory (DFT) provides the theoretical prediction of molecular stability and reactivity which are essential factors

* Corresponding author.
*E-mail address:* sujamystica@yahoo.com (S.P. Jose).

https://doi.org/10.1016/j.heliyon.2019.e02149
Received 30 October 2018; Received in revised form 17 May 2019; Accepted 22 July 2019

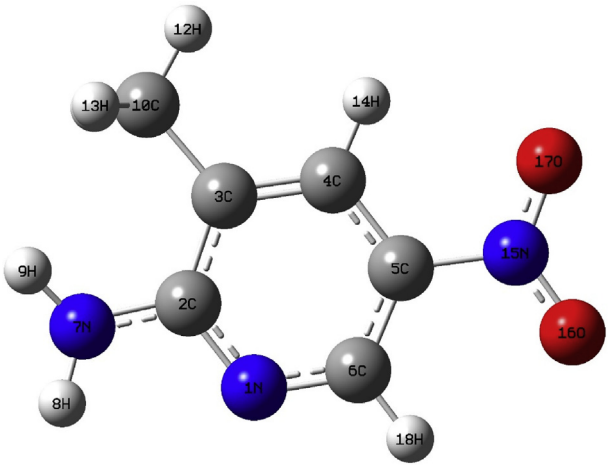


**Fig. 1.** The optimized geometry of the 2A3M5NP molecule at DFT/B3LYP level cc-pVTZ basis set.

in the arena of molecular drug designing and helps us to understand the chemical mechanism in biological systems [14, 15]. The compound, 2A3M5NP is a derivative of pyridine and to our best knowledge, no quantum chemical investigations were carried out for this compound. Considering all these aspects and the importance of the title compound 2A3M5NP, an attempt has been made to present a complete molecular geometry, vibrational analysis and other related properties of 2A3M5NP with the aid of quantum chemical calculations along with experimental results. The density functional theory (DFT) calculations have also been carried out to support the accuracy of wavenumber assignments. Detailed interpretation of the vibrational spectra has also been done in the present work which is validated with the calculation of potential energy distribution (PED).

## 2. Experimental

The compound, 2-amino-3-methyl-5-nitropyridine (2A3M5NP) in solid form was purchased from Sigma Aldrich (USA) with purity greater than 99%. The compound is used as such without any further purifications. The FT-Raman spectrum of the compound is recorded in the region from 4000 - 100 $cm^{-1}$ using BRUKER RFS 27 FT-Raman spectrometer with 1064 nm Nd:YAG laser source with a spectral resolution of 2 $cm^{-1}$. The Fourier transform infrared spectrum of 2A3M5NP is investigated at room temperature in the region 4000-400 $cm^{-1}$ using KBr method on Shiraz FTIR spectrometer. The UV-Visible absorption spectrum was recorded in the region 200–800 nm with ethanol as a solvent in SHIMADZU UV-2450 spectrophotometer.

## 3. Theory/calculation

All the quantum chemical investigations of 2A3M5NP are performed using density functional theory (DFT) by Gaussian 03 program [16]. The geometries of 2A3M5NP are optimized with the B3LYP-exchange-correlation functional with 6-311G (d,p), 6-311G++(d,p) and cc-pVTZ basis sets. The DFT vibrational wavenumbers are calculated for the lowest energy basis sets, cc-pVTZ to confirm the absence of imaginary frequencies. The modes of vibrations are assigned by comparing the experimental results with the graphical interface GaussView 5 program [17]. The electronic properties of the molecule are studied using time-dependent density functional theory (TD-DFT) and isodensity polarizable continuum model (I-PCM). Investigations of various vibrational parameters and the PED calculations are done by VEDA 4 program [18] and the consistency of the experimental and theoretical values are achieved by using different scaling factors.

**Table 1**
The computed bond lengths (Å) of 2A3M5NP molecule at DFT/B3LYP 6-311G (d,p), 6-311G++(d,p) and cc-pVTZ basis sets.

| Bond length (Å) | Theoretical | | | Experimental[a] |
|---|---|---|---|---|
| | 6-311G (d,p) | 6-311G++(d,p) | cc-pVTZ | |
| N1–C2 | 1.343 | 1.343 | 1.340 | 1.35 |
| N1–C6 | 1.328 | 1.328 | 1.325 | 1.34 |
| C2–C3 | 1.424 | 1.424 | 1.420 | 1.41 |
| C2–N7 | 1.364 | 1.364 | 1.361 | 1.31 |
| C3–C4 | 1.379 | 1.379 | 1.376 | 1.34 |
| C3–C10 | 1.504 | 1.504 | 1.501 | - |
| C4–C5 | 1.397 | 1.398 | 1.394 | 1.40 |
| C4–H14 | 1.082 | 1.082 | 1.080 | 0.93 |
| C5–C6 | 1.389 | 1.390 | 1.386 | 1.33 |
| C5–N15 | 1.458 | 1.457 | 1.455 | 1.44 |
| C6–H18 | 1.083 | 1.083 | 1.080 | 0.93 |
| N7–H8 | 1.007 | 1.007 | 1.005 | 0.88 |
| N7–H9 | 1.005 | 1.005 | 1.002 | 0.87 |
| C10–H11 | 1.095 | 1.095 | 1.093 | - |
| C10–H12 | 1.090 | 1.090 | 1.088 | - |
| C10–H13 | 1.096 | 1.096 | 1.094 | - |
| N15–O16 | 1.226 | 1.228 | 1.225 | 1.22 |
| N15–O17 | 1.227 | 1.229 | 1.226 | 1.25 |

[a] Ref [19].

**Table 2**
The computed bond angles (°) of 2A3M5NP molecule at DFT/B3LYP 6-311G (d,p), 6-311G++(d,p) and cc-pVTZ basis sets.

| Bond angle (°) | Theoretical | | | Experimental[a] |
|---|---|---|---|---|
| | 6-311G (d,p) | 6-311G++(d,p) | cc-pVTZ | |
| C2–N1–C6 | 118.4 | 118.6 | 118.6 | 122.9 |
| N1–C2–C3 | 123.4 | 123.4 | 123.3 | 117.3 |
| N1–C2–N7 | 115.5 | 115.5 | 115.6 | 119.3 |
| C3–C2–N7 | 120.9 | 120.9 | 120.8 | 123.4 |
| C2–C3–C4 | 116.7 | 116.7 | 116.7 | 120.3 |
| C2–C3–C10 | 120.8 | 121.0 | 120.9 | - |
| C4–C3–C10 | 122.3 | 122.2 | 122.3 | - |
| C3–C4–C5 | 119.4 | 119.5 | 119.5 | 118.9 |
| C3–C4–H14 | 121.3 | 121.1 | 121.2 | 120.5 |
| C5–C4–H14 | 119.1 | 119.2 | 119.2 | 120.5 |
| C4–C5–C6 | 119.5 | 119.6 | 119.5 | 120.7 |
| C4–C5–N15 | 120.1 | 120.1 | 120.1 | 119.4 |
| C6–C5–N15 | 120.2 | 120.2 | 120.2 | 119.8 |
| N1–C6–C5 | 122.1 | 122.0 | 122.0 | 119.6 |
| N1–C6–H18 | 117.6 | 117.5 | 117.6 | 120.2 |
| C5–C6–H18 | 120.1 | 120.3 | 120.2 | 120.2 |
| C2–N7–H8 | 116.2 | 116.9 | 116.6 | 122.1 |
| C2–N7–H9 | 120.8 | 121.1 | 120.7 | 124.1 |
| H8–N7–H9 | 117.8 | 118.0 | 117.9 | 114.0 |
| C3–C10–H11 | 111.3 | 111.4 | 111.4 | - |
| C3–C10–H12 | 110.9 | 110.8 | 110.9 | - |
| C3–C10–H13 | 111.6 | 111.7 | 111.6 | - |
| H11–C10–H12 | 107.8 | 107.7 | 107.8 | - |
| H11–C10–H13 | 107.4 | 107.5 | 107.3 | - |
| H12–C10–H13 | 107.4 | 107.3 | 107.4 | - |
| C5–N15–O16 | 117.8 | 117.9 | 117.9 | 116.7 |
| C5–N15–O17 | 117.6 | 117.7 | 117.7 | 119.0 |
| O16–N15–O17 | 124.5 | 124.3 | 124.3 | 122.5 |

[a] Ref [19].

## 4. Results and discussion

### 4.1. Molecular geometry

The title compound contains a nitro group, a methyl group and an amine group attached with pyridine ring. The energies of the title compound, 2A3M5NP are investigated by DFT/B3LYP level with different basis sets 6-311G (d,p), 6-311G++ (d,p) and cc-pVTZ. The corresponding energies are -547.617, -547.632 and -547.675 a. u respectively. The computed optimized geometry of 2A3M5NP possesses a $C_1$ point group

**Table 3**
Experimental and calculated frequencies of 2A3M5NP by DFT/B3LYP method with cc-pVTZ basis set.

| S.No | Experimental | | Theoretical | | IR Intensity | Raman Activity | Raman Intensity | % PED assignments |
|---|---|---|---|---|---|---|---|---|
| | FT-IR ($cm^{-1}$) | FT-Raman ($cm^{-1}$) | Unscaled ($cm^{-1}$) | Scaled ($cm^{-1}$) | | | | |
| 1 | 3451 vs | 3456vw | 3727 | 3444 | 44.37 | 56.43 | 59.73 | $\nu_{as}$ NH (100) |
| 2 | 3320 s | - | 3599 | 3326 | 94.88 | 248.33 | 297.27 | $\nu_{s}$ NH (100) |
| 3 | 3262 w | - | 3211 | 3113 | 1.97 | 47.18 | 83.07 | N CH (99) |
| 4 | 3127 s | 3063 vw | 3199 | 3102 | 0.21 | 70.82 | 126.17 | N CH (100) |
| 5 | 2943 w | 2946 w | 3113 | 3018 | 9.33 | 55.30 | 107.66 | $\nu_{as}$ CH (90) |
| 6 | 2915 w | 2916 w | 3051 | 2958 | 16.39 | 90.07 | 187.01 | $\nu_{as}$ CH (99) |
| 7 | 2857 m | - | 3009 | 2917 | 27.10 | 220.74 | 478.74 | $\nu_{s}$ CH (91) |
| 8 | - | - | 1651 | 1639 | 358.47 | 59.41 | 698.60 | ν CC (27) + β HNH (33) |
| 9 | 1652 vs | 1661 vs | 1633 | 1621 | 73.97 | 6.96 | 84.24 | δ HNH (29) |
| 10 | - | 1601 s | 1623 | 1611 | 110.90 | 18.65 | 229.16 | νCC (24) + β HNH (17) |
| 11 | 1586 vs | 1580 s | 1567 | 1555 | 129.14 | 17.07 | 229.24 | ν NO (63) |
| 12 | - | 1491 m | 1513 | 1501 | 29.10 | 6.70 | 98.27 | β HCH (79) |
| 13 | 1481 s | 1476 m | 1489 | 1478 | 8.28 | 7.63 | 116.54 | δ HNH (79) + τ HCCC (14) |
| 14 | - | - | 1478 | 1467 | 104.70 | 14.12 | 219.76 | ν CN (19) + β HCH (15) |
| 15 | - | - | 1462 | 1451 | 13.94 | 14.26 | 228.09 | ν CN (19) + ν CC (33) + β HCN (11) |
| 16 | 1422 m | 1415 m | 1422 | 1411 | 6.03 | 8.35 | 142.99 | δ HCH (87) |
| 17 | 1346 s | 1351 s | 1365 | 1355 | 513.96 | 287.54 | 5443.03 | ν NO (62) + β ONO (12) |
| 18 | - | 1341 m | 1357 | 1347 | 76.12 | 37.01 | 710.37 | ν CN (51) + β HCN (17) |
| 19 | - | - | 1343 | 1333 | 99.29 | 132.59 | 2610.82 | ν CN (43) + ν CC (14) + β HNC (10) |
| 20 | 1291 m | 1296 vs | 1295 | 1285 | 19.27 | 11.19 | 240.99 | β HCC (33) + β HCN (35) |
| 21 | 1263 w | 1210 w | 1223 | 1214 | 27.36 | 23.83 | 587.87 | ν CC (27) + β CCC (29) |
| 22 | 1105 m | 1104 m | 1125 | 1116 | 73.29 | 17.90 | 538.72 | ν CC (27) + ν CN (12) + β HCC (31) |
| 23 | - | - | 1071 | 1063 | 1.43 | 0.04 | 1.58 | β HCH (22) + τ HCCC (74) |
| 24 | 1036 m | 1054 m | 1047 | 1039 | 4.15 | 4.48 | 159.84 | ν CN (23) + β HNC (46) |
| 25 | 1008 m | - | 1019 | 1011 | 10.54 | 3.89 | 147.67 | β HCH (11) + τ HCCC (52) |
| 26 | - | 958 m | 982 | 974 | 6.01 | 0.95 | 39.53 | τ HCNC (78) + τ CNCC (12) |
| 27 | 938 w | - | 976 | 968 | 8.27 | 10.76 | 452.02 | ν CC (28) + ν CN (13) |
| 28 | 916 w | - | 954 | 947 | 6.59 | 0.45 | 20.19 | τ HCCC (71) + τ CCCC (10) |
| 29 | 824 w | 828 m | 843 | 836 | 18.83 | 1.56 | 91.52 | δ ONO (41) + β CNC (10) + β CCC (14) |
| 30 | - | 776 m | 796 | 790 | 21.37 | 0.74 | 49.72 | τ CNCC (13) + γ OCON (13) + γ NCNC (33) |
| 31 | 768 m | - | 779 | 773 | 8.72 | 25.65 | 1794.28 | ν CC (14) + ν CN (11) + β ONO (11) + β NCC (15) |
| 32 | 742 m | - | 768 | 762 | 3.62 | 1.12 | 81.00 | γ OCON (70) |
| 33 | 657 m | 656 vw | 661 | 656 | 6.80 | 2.06 | 207.77 | ν CC (10) + β CNC (12) + β ONO (12) + β NCC (13) + β CCC (22) |
| 34 | 558 s | 553 vw | 562 | 557 | 3.74 | 1.39 | 200.10 | β ONC (43) + β NCC (12) |
| 35 | - | - | 553 | 548 | 5.64 | 2.74 | 409.52 | ν CC (10) + β CCC (12) + τ HNCC (10) + τ NCCC (11) + γ NCNC (14) |
| 36 | 532 m | - | 551 | 546 | 2.93 | 1.80 | 270.71 | τ HNCC (61) + γ CCCC (10) |
| 37 | - | - | 529 | 525 | 22.00 | 1.51 | 249.12 | β ONC (78) |
| 38 | 442 w | 442vw | 441 | 437 | 2.65 | 0.10 | 26.53 | τ HNCC (13) + τ CCCC (26) + τ CNCC (16) + γ CCCC (26) |
| 39 | 423 m | - | 425 | 421 | 1.70 | 2.78 | 731.62 | β ONC (26) + β NCN (29) + β CCC (17) |
| 40 | - | - | 368 | 365 | 1.72 | 3.17 | 1126.43 | ν CN (40) + β CNC (16) + β ONO (11) |
| 41 | - | - | 328 | 325 | 35.00 | 0.63 | 286.68 | τ CNCC (10) + γ NCCC (28) + γ NCNC (15) + γ CCCC (23) |
| 42 | - | - | 307 | 304 | 4.74 | 1.76 | 919.64 | β NCN (21) + β CCC (45) |
| 43 | - | - | 282 | 280 | 209.39 | 4.38 | 2719.20 | τ HNCC (84) |
| 44 | - | - | 205 | 203 | 1.17 | 0.39 | 482.09 | β ONC (13) + β CCC (11) + β NCC (62) |
| 45 | - | - | 190 | 188 | 9.34 | 0.57 | 817.51 | τ HCCC (76) + γ NCCC (13) |
| 46 | - | - | 182 | 180 | 0.44 | 0.40 | 629.32 | τ NCCC (24) + τ CNCC (13) + γ NCCC (15) + γ CCCC (26) |
| 47 | - | - | 105 | 104 | 0.22 | 0.96 | 4526.10 | τ NCCC (46) + τ CCCC (18) + γ NCCC (22) |
| 48 | - | - | 61 | 60 | 0.09 | 0.16 | 2424.41 | τ ONCC (90) |

vs – very strong, s – strong, m – medium, w - weak, vw – very weak, b – broad, ν – stretching, $\nu_{as}$ – asymmetric stretching, $\nu_{s}$– symmetric stretching, β-in plane bending, τ-torsional, γ-out of plane bending, δ-scissoring/deformation, ω – wagging.

symmetry. The optimised structure of 2A3M5NP compound using DFT/B3LYP level with cc-pVTZ basis set is given in Fig. 1. The computed geometrical parameters like bond length and bond angles are listed in Table 1 and Table 2. The computed geometrical parameters are compared with X-ray data of closely related molecule 2-amino-5-nitropyridinium sulfamate [19]. From structural data, it is observed that various bond distances of the title compound are found to be same for all level calculations. The introduction of polarization and diffusion functions show no significant changes in bond distances and bond angles. From X-ray diffraction studies of pyridine compound, it is found that C–C bond distances are 1.39 Å and C–N bond distances are 1.37 Å. The ring C–C bond distances are similar to pyridine compound except for C2–C3 = 1.420 Å. This is due to the introduction of methyl group at C3 and amine group at C2. The steric repulsion between the methyl group and amine group leads to distortion for C–C bond distance. The variation between bond distances N1–C2 = 1.34 Å and N1–C6 = 1.32 Å shows the ring C–N bond distances distort and leads to delocalization of electrons in the ring.

### 4.2. Vibrational analysis

The molecule, 2A3M5NP consists of 18 atoms and have (3N-6), that is 48 normal modes of vibration which are both IR and Raman active. The neglect of anharmonicity, incomplete treatment of electron-correlation functional and deficiency of basis sets lead to the theoretically predicted frequencies overestimated than the experimentally observed frequencies [20]. The scaling factor is introduced to improve a good

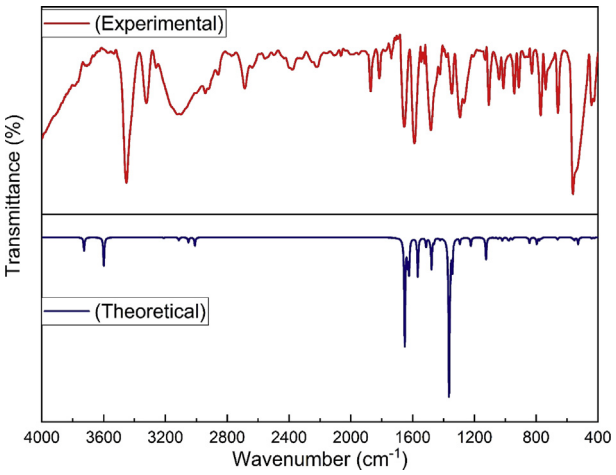


**Fig. 2.** The combined theoretical and experimental FTIR spectra of 2A3M5NP molecule.

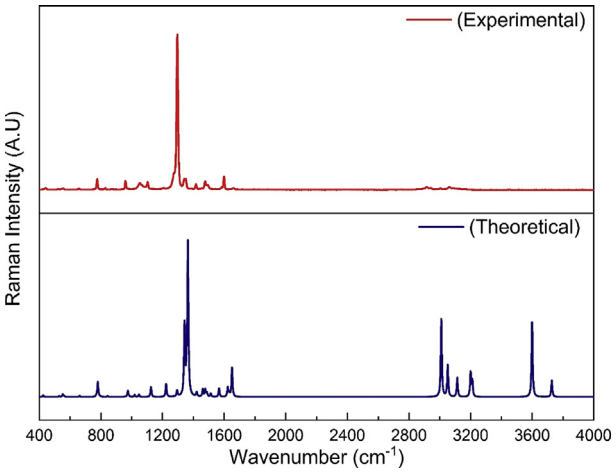


**Fig. 3.** The combined theoretical and experimental FT-Raman spectra of 2A3M5NP molecule.

agreement between the predicted frequencies and observed frequencies. The region below 1800 $cm^{-1}$ is termed as the fingerprint region and the region has large density of states leads to congestion of absorption peaks. So a special attention is given to this region. In the present work, different scaling factors were introduced [21, 22]. The scaling factors 0.9242, 0.9697 and 0.9927 are used for N–H stretching, C–H stretching and other modes respectively. The scaling factor (λ) is calculated from the equation,

$$\lambda = \frac{\sum_i^N \left(\nu_{cal} * \nu_{exp}\right)}{\sum_i^N \left(\nu_{cal}\right)^2} \quad (1)$$

where N is the number of vibrational modes, $\nu_{cal}$ and $\nu_{exp}$ are the calculated and the experimental wavenumbers respectively.

The vibrational assignments of 2A3M5NP molecule have been made by using GaussView software and the potential energy distribution (PED) calculations are carried out by using VEDA software. The vibrational assignments of 2A3M5NP along with IR intensity, Raman activity, Raman intensity and potential energy distributions are shown in Table 3. The combined experimental and theoretical FTIR and FT-Raman spectra of 2A3M5NP are shown in Fig. 2 and Fig. 3.

#### 4.2.1. $NH_2$ vibrations

The primary amines give rise to six modes of vibrations namely asymmetric stretching, symmetric stretching, deformation, rocking, wagging and torsional. In primary amine, the N–H stretching modes are expected in the region 3500-3300 $cm^{-1}$ [23,24]. The symmetric and asymmetric modes are associated with an empirical relationship [25], and from this equation, it is confirmed that the asymmetric mode is always higher in wavenumber than the symmetric mode of vibration.

$$\nu_{sym} = 345.5 + 0.876\ \nu_{asym} \quad (2)$$

In the present study, the asymmetric N–H stretching mode of vibration is observed at 3451 $cm^{-1}$ in FTIR with very strong intensity while in FT-Raman spectrum, the peak is observed with very weak intensity at 3456 $cm^{-1}$. The symmetric N–H stretching mode of vibration is observed at 3320 $cm^{-1}$in FTIR with strong intensity. The $NH_2$ deformation or scissoring mode of vibration usually falls in the range 1650–1580 $cm^{-1}$ [25,26]. In case of 4-amino-2-methylquinoline, the vibrational mode at 1659 $cm^{-1}$ is assigned to $NH_2$ deformation mode [27]. In the present work, the very strong intensity absorption peak observed at 1652 $cm^{-1}$ in FTIR and 1661 $cm^{-1}$in FT-Raman are assigned to $NH_2$ deformation modes. The corresponding calculated wavenumbers agree well with the observed ones. The $NH_2$ rocking mode is observed at 1036 $cm^{-1}$ in FTIR and at 1054 $cm^{-1}$ in FT-Raman. The $NH_2$ wagging mode usually appears to be in the range from 910 $cm^{-1}$ to 665 $cm^{-1}$ [28,29]. In present work, the $NH_2$ wagging mode and the $NH_2$ twisting mode are absent in both FTIR and FT-Raman spectra. The wagging mode is assigned to 282 $cm^{-1}$ from the DFT computed result.

#### 4.2.2. $CH_3$ vibrations

The methyl group is associated with seven vibrational modes namely asymmetric stretching, symmetric stretching, asymmetric deformation, symmetric deformation, rocking, wagging and twisting. The absorption of methyl group results in a medium to strong intensity bands in the region 3000-2800 $cm^{-1}$ for both IR and FT-Raman [25]. The asymmetric C–H stretching is expected in the region 3010-2900 $cm^{-1}$ whereas, the symmetric C–H stretching around 2950-2850 $cm^{-1}$ [30]. The position of the symmetric C–H stretching may change due to the presence of the adjacent group in the molecule and the presence of electronegative atoms or groups adjacent can alter the methyl symmetric band significantly [25]. In 4-Bromomethyl-5-methyl-1,3-dioxol-2-one, CH vibrational modes occur at 3034 $cm^{-1}$, 2927 $cm^{-1}$ in FTIR and at 3035$cm^{-1}$, 2924 $cm^{-1}$ in FT-Raman are assigned to asymmetric C–H stretching vibrations [31]. In the present work, medium intensity FTIR absorption peaks at 2943 $cm^{-1}$ and 2915 $cm^{-1}$ and very weak intensity FT-Raman absorption peaks at 2946 $cm^{-1}$ and 2916 $cm^{-1}$ are assigned to asymmetric $CH_3$ stretching mode and the medium intensity FTIR absorption peak at 2857 $cm^{-1}$ is assigned to symmetric $CH_3$ stretching mode. The asymmetric methyl deformation modes occur in the region 1470-1400 $cm^{-1}$ with medium to strong intensity whereas, the symmetric $CH_3$ deformation modes are expected near 1370 $cm^{-1}$ [24]. In the present work, the strong intensity absorption peak arises at 1481 $cm^{-1}$ in FTIR and the medium intense peak at 1476 $cm^{-1}$ in FT-Raman are assigned to asymmetric methyl group deformation modes. The medium intense peak at 1422 $cm^{-1}$ in FTIR and 1415 $cm^{-1}$ in FT-Raman are assigned to symmetric methyl group deformation modes of vibration. The shift in the frequency is due to the presence of the amine and nitro group within the molecule. The $CH_3$ rocking and wagging modes are assigned from the DFT computed wavenumbers. These assignments are compared with literatures [32, 33, 34].

#### 4.2.3. $NO_2$ vibrations

The nitro group attached to the pyridine ring constitutes asymmetric stretching, symmetric stretching, deformation, wagging, rocking, twisting modes of vibrations. The asymmetric and symmetric stretching modes of nitro group are expected in the regions 1570-1485 $cm^{-1}$ and 1370-1320 $cm^{-1}$ respectively [25]. From literature, the asymmetric modes are found around 1530 $cm^{-1}$ whereas the symmetric stretching mode are observed around 1350 $cm^{-1}$ in FTIR as well as in FT-Raman

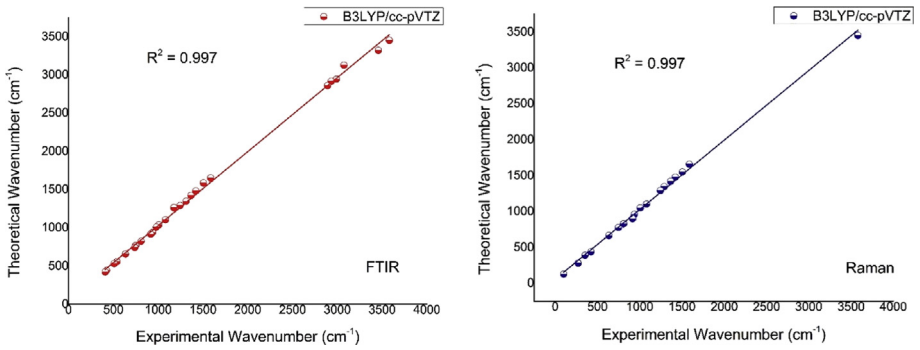


**Fig. 4.** The correlation diagram for the experimental and theoretical wavenumbers of 2A3M5NP molecule.

spectrum [35, 36, 37]. The methyl group which is a part of the molecular system acts as an electron donating group and further leads to some shifts in vibrational modes of nitro group [37].

In the present work, the asymmetric stretching of nitro group is observed as strong intensity band at 1586 $cm^{-1}$ in FTIR and at 1580 $cm^{-1}$ in FT-Raman spectrum. The symmetric stretching mode is observed at 1346 $cm^{-1}$ and 1351 $cm^{-1}$ in FTIR and FT-Raman spectrum respectively. The deformation mode of nitro group is expected around 850 $cm^{-1}$. Here, the $NO_2$ deformation modes are assigned to 824 $cm^{-1}$ in FTIR and 828 $cm^{-1}$ in FT-Raman spectrum. The $NO_2$ wagging mode is observed at 742 $cm^{-1}$ in FTIR. A strong intense absorption peak found in FTIR spectrum is assigned to the rocking mode of $NO_2$. The twisting mode is very difficult to find out in both the FTIR and FT-Raman spectra and hence they are predicted from DFT calculations. All the vibrational modes are compared with the theoretical frequencies calculated from DFT.

#### 4.2.4. C–H vibrations

The C–H stretching vibrations of aromatic compounds show absorption bands in the region 3100-3000 $cm^{-1}$ [25]. The band in this region is not affected by the nature of substituents. According to the literature survey, the FTIR spectrum shows a medium to strong intensity bands whereas the FT-Raman spectrum shows strong intensity bands. In this work, the molecule 2A3M5NP consists of two C–H groups in the ring corresponding to two C–H stretching modes, two in-plane bending modes and two out of plane bending modes of vibrations respectively. The medium and strong intensity absorption peaks located at 3262 $cm^{-1}$ and 3127 $cm^{-1}$ in FTIR spectrum is assigned to C–H stretching vibrations. These modes are absent in FT-Raman spectrum. The increase in the wavenumber is due to the inductive/mesomeric effect of the substituent in the ring. The C–H in-plane bending vibrations for pyridine compound are expected in the regions 1300-1180 $cm^{-1}$ and 1100-1000 $cm^{-1}$ [38]. A medium intensity FTIR peak at 1290 $cm^{-1}$, 1105 $cm^{-1}$ and strong intensity FT-Raman peaks at 1296 $cm^{-1}$, 1104 $cm^{-1}$ are assigned to C–H in-plane bending vibrations and these modes are exactly agreeing with the theoretically calculated wavenumbers 1285 $cm^{-1}$ and 1116 $cm^{-1}$. The number of adjacent hydrogens in the aromatic ring decides the number of C–H out of plane bending modes. These C–H out of plane bending modes of pyridine ring are located in the region 1000 to 700 $cm^{-1}$ [39]. The experimental FTIR peak at 916 $cm^{-1}$ and FT-Raman peaks at 958 $cm^{-1}$ are assigned to C–H out of plane bending vibrations.

#### 4.2.5. C–C, C–N, C–$NH_2$, C–$CH_3$, C–$NO_2$ vibrations

The interaction between ring C–C and C–N stretching vibrations results in two strong to medium intense absorption peaks about 100 $cm^{-1}$ apart. The separation of C–N vibrational modes is simply a difficult task because it intermixes with other C–C vibrational modes [29]. For pyridine molecule, these vibrational modes occur over the regions 1615-1575 $cm^{-1}$ and 1520-1465 $cm^{-1}$ [40]. In the present work, there are no significant absorption peaks due to the substitutions. All the C–C and C–N stretching modes were calculated from DFT results. The stretching C–$NH_2$ vibrations appeared at 1341 $cm^{-1}$ in FT-Raman spectrum with medium intensity. The in-plane C–$NH_2$ bending mode has appeared at 423 $cm^{-1}$ of FTIR spectrum. The stretching C–$CH_3$ vibrations appeared at 1263 $cm^{-1}$ in FTIR spectrum with medium intensity. All the assignments agree well with literature values [34, 41].

#### 4.2.6. Ring breathing vibration

The ring breathing of pyridine and pyridine derivatives is found in the region 900-750 $cm^{-1}$ [34]. In the present work, the vibrational mode observed at 768 $cm^{-1}$in FTIR is assigned to ring breathing mode. The error distribution of the scaled, calculated vibrational frequencies and experimentally observed frequencies were given with the help of histogram. By implementing different scaling factors for different functional groups leads to minimizing the errors between scaled and experimental frequencies. The root-mean square (RMS) deviation is evaluated and the correlation coefficient R is calculated for the compound. These RMS value helps to understand the appreciable errors between theoretical and experimental wavenumbers.

$$\mathrm{RMS} = \frac{1}{n-1}\sum_{i}^{n}\left(\vartheta_i^{cal} - \vartheta_i^{exp}\right)^2 \quad (3)$$

An error of 14.33 for FTIR and 8.01 for FT-Raman data is observed from RMS value and the error may be due to the fact that the experimental data is taken in solid phase whereas the computed data is in the gaseous phase. The correlation diagram of FTIR and FT-Raman is given in Fig. 4.

### 4.3. Natural bonding orbital analysis

Natural bonding orbital (NBO) analysis provides an efficient theoretical information about intra and intermolecular charge transfer (ICT) and a valuable information about conjugation and hyperconjugation of the molecular system. The analysis also provides the nature of bonds and their hybridization based on the electron occupancy between the corresponding bonds [42]. The delocalization effect of the electrons in the molecular system can be identified by analysing the second order perturbation results provided by the NBO 3.1 program [43]. The Fock matrix analysis provides the information about donor-acceptor orbitals interaction and their stabilization energies and the energy E (2) represents the off-diagonal NBO Fock matrix element

$$E(2) = \Delta E_{ij} = q_i \frac{(F_{ij})^2}{(E_j - E_i)} \quad (4)$$

where $q_i$ is the donor orbital occupancy, $F_{ij}$ is the donor-acceptor interaction and $E_j$ and $E_i$ are the donor and the acceptor orbital energies respectively. The π type orbitals are weaker than the σ type orbitals resulting in lowering of electron occupancy with associated atoms [44]. Second order perturbation theory analysis of Fock matrix of 2A3M5NP using NBO analysis is presented in Table 4.

**Table 4**
Second order perturbation theory analysis of Fock matrix on NBO basis for 2A3M5NP at B3LYP/cc-pVTZ basis set.

| Donor (i) | ED/e | Acceptor (j) | [a]$E^{(2)}$ kcal/mol | [b]E(j)-E(i) a.u. | [c]F (i,j) a.u. |
|---|---|---|---|---|---|
| σ (N1–C2) | 1.98266 | σ* (C2–C3) | 2.25 | 1.32 | 0.049 |
| | | σ* (C3–C10) | 2.38 | 1.21 | 0.048 |
| | | σ* (C6–H18) | 2.29 | 1.24 | 0.048 |
| | | σ* (N7–H9) | 2.09 | 1.24 | 0.045 |
| π (N1–C2) | 1.67863 | π* (C3–C4) | 9.15 | 0.33 | 0.05 |
| | | π* (C5–C6) | 33.56 | 0.32 | 0.093 |
| σ (N1–C6) | 1.98356 | σ* (C2–N7) | 4.13 | 1.28 | 0.065 |
| | | σ* (C5–N15) | 2.98 | 1.13 | 0.053 |
| σ (C2–C3) | 1.97574 | σ* (C3–C4) | 2.07 | 1.26 | 0.046 |
| | | σ* (C4–H14) | 3.22 | 1.12 | 0.054 |
| | | σ* (N7–H8) | 2.32 | 1.11 | 0.046 |
| σ (C2–N7) | 1.99088 | σ* (N1–C6) | 2.83 | 1.37 | 0.056 |
| σ (C3–C4) | 1.97354 | σ* (C2–C3) | 2.02 | 1.21 | 0.044 |
| | | σ* (C2–N7) | 3.88 | 1.16 | 0.06 |
| | | σ* (C4–C5) | 2.3 | 1.25 | 0.048 |
| | | σ* (C5–N15) | 4.35 | 1.01 | 0.06 |
| π (C3–C4) | 1.70667 | π* (N1–C2) | 28.12 | 0.26 | 0.08 |
| | | π* (C5–C6) | 14.67 | 0.28 | 0.058 |
| | | π* (C10–H11) | 3.03 | 0.63 | 0.042 |
| | | π* (C10–H13) | 3.22 | 0.63 | 0.043 |
| σ (C3–C10) | 1.98182 | σ* (N1–C2) | 3.45 | 1.15 | 0.056 |
| | | σ* (C3–C4) | 2.13 | 1.2 | 0.045 |
| | | σ* (C4–C5) | 2.89 | 1.17 | 0.052 |
| σ (C4–C5) | 1.97639 | σ* (C3–C4) | 2.2 | 1.27 | 0.047 |
| | | σ* (C3–C10) | 4.58 | 1.09 | 0.063 |
| | | σ* (C5–C6) | 3.23 | 1.24 | 0.057 |
| | | σ* (C6–H18) | 2.25 | 1.13 | 0.045 |
| | | σ* (N15–O16) | 2.31 | 1.14 | 0.046 |
| σ (C4–H14) | 1.97356 | σ* (C2–C3) | 5.07 | 1.02 | 0.064 |
| | | σ* (C5–C6) | 4.55 | 1.06 | 0.062 |
| σ (C4–C6) | 1.98293 | σ* (C4–C5) | 3.28 | 1.24 | 0.057 |
| | | σ* (C4–H14) | 2.53 | 1.14 | 0.048 |
| | | σ* (N15–O17) | 2.34 | 1.15 | 0.047 |
| π (C5–C6) | 1.64619 | π* (N1–C2) | 11.95 | 0.26 | 0.051 |
| | | π* (C3–C4) | 23.41 | 0.3 | 0.076 |
| | | π* (N15–O16) | 28.9 | 0.15 | 0.064 |
| σ (C5–N15) | 1.9896 | σ* (N1–C6) | 1.7 | 1.33 | 0.042 |
| | | σ* (C3–C4) | 1.74 | 1.35 | 0.043 |
| | | σ* (C4–C5) | 0.73 | 1.32 | 0.028 |
| | | σ* (C5–C6) | 0.61 | 1.33 | 0.026 |
| σ (C6–H18) | 1.97543 | σ* (N1–C2) | 6.01 | 1.03 | 0.07 |
| | | σ* (C4–C5) | 4.6 | 1.04 | 0.062 |
| σ (N7–H8) | 1.98863 | σ* (C2–C3) | 4.67 | 1.16 | 0.066 |
| σ (N7–H9) | 1.98802 | σ* (N1–C2) | 3.88 | 1.19 | 0.061 |
| σ (C10–H11) | 1.97911 | σ* (C3–C4) | 2.45 | 1.07 | 0.046 |
| | | σ* (C3–C4) | 3.24 | 0.54 | 0.04 |
| σ (C10–H12) | 1.98696 | σ* (C2–C3) | 5.44 | 1 | 0.067 |
| σ (C10–H13) | 1.97859 | σ* (C3–C4) | 2.3 | 1.07 | 0.044 |
| | | σ* (C3–C4) | 3.31 | 0.54 | 0.04 |
| σ (N15–O16) | 1.99563 | σ* (C4–C5) | 1.15 | 1.59 | 0.038 |
| π (N15–O16) | 1.98639 | π* (C5–C6) | 3.07 | 0.45 | 0.036 |
| | | π* (N15–O16) | 7.82 | 0.32 | 0.054 |
| σ (N15–O17) | 1.99589 | σ* (C5–C6) | 1.04 | 1.59 | 0.037 |
| | | σ* (C5–N15) | 0.51 | 1.35 | 0.024 |
| n (N1) | 1.90505 | σ* (C2–C3) | 13.14 | 0.84 | 0.095 |
| | | σ* (C2–N7) | 4 | 0.79 | 0.051 |
| | | σ* (C5–C6) | 11.22 | 0.88 | 0.09 |
| | | σ* (C6–H18) | 3.94 | 0.76 | 0.05 |
| n (N7) | 1.76357 | π* (N1–C2) | 47.02 | 0.28 | 0.108 |
| n (O16) | 1.97976 | σ* (C5–N15) | 4.69 | 1.07 | 0.065 |
| | | σ* (N15–O17) | 2.84 | 1.21 | 0.053 |
| n (O16) | 1.89609 | σ* (C5–N15) | 14.7 | 0.56 | 0.081 |
| | | σ* (N15–O17) | 19.5 | 0.7 | 0.106 |
| n (O17) | 1.97983 | σ* (C5–N15) | 4.61 | 1.07 | 0.064 |
| | | σ* (N15–O16) | 2.81 | 1.21 | 0.053 |
| n (O17) | 1.89652 | σ* (C5–N15) | 14.69 | 0.57 | 0.081 |
| | | σ* (N15–O16) | 19.33 | 0.71 | 0.106 |
| n (O17) | 1.46425 | π* (N15–O16) | 160.85 | 0.14 | 0.139 |

[a] $E^{(2)}$ means energy for hyperconjugative energy (stabilization energy).
[b] Energy difference between donor (i) and acceptor (j) NBO orbitals.
[c] F (i,j) is the Fock matrix element between i & j NBO orbitals.

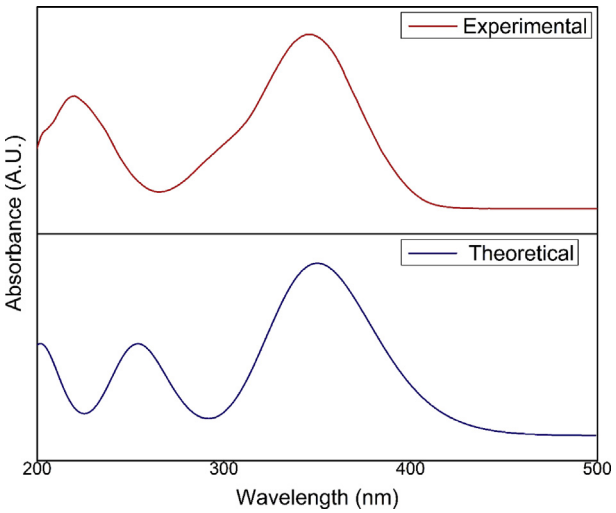


**Fig. 5.** The observed and calculated absorbance spectra of 2A3M5NP molecule in ethanol.

**Table 5**
The calculated and experimental UV-visible parameters of 2A3M5NP molecule.

| Experimental Wavelength λ (nm) in ethanol | Transition | Calculated with B3LYP/cc-pVTZ level in ethanol | | |
|---|---|---|---|---|
| | | λ max (nm) | Excitation energy (eV) | f (Oscillator strength) |
| 220 | π → π* | 253.62 | 4.8886 | 0.1814 |
| 345 | n → π* | 350.03 | 3.5421 | 0.3545 |

In the present work, the electron occupancy of σ bonds and π bonds are in the range of 1.97354e to 1.99589e and 1.64619e to 1.98639e for 2A3M5NP molecule. The Lewis bonding donor orbital π(N1–C2) interacts with non-Lewis anti-bonding acceptor orbital π*(C5–C6) with a strong delocalization energy of 33.56 kcal/mol rather than π*(C3–C4) orbital. The bonding orbital π(C5–C6) interacts with non-bonding orbital π*(N15–O16) with greater stabilization energy of 28.90 kcal/mol. The Lewis bonding donor orbital π(C3–C4) interacts with non-Lewis anti-bonding acceptor orbitals π*(N1–C2) and π*(C5–C6) with a delocalization energy of 28.12 kcal/mol and 14.67 kcal/mol respectively. The delocalization of electrons favours π*(N1–C2) greatly due to the presence of electronegative atom. Concerning about the lone pair electrons delocalization, the lone pair electrons of the amine group nitrogen n (N7) leads to a strong interaction with π*(N1–C2) with a strong stabilization energy of 47.02 kcal/mol. In the nitro group, the lone pair electrons of n (O17) lead to a strong interaction with π*(N15–O16) with a strong delocalization energy of 160.85 kcal/mol. The positive (+M) and negative (-M) mesomeric effect of the amine group and the nitro group act as an electron donor and electron acceptor respectively [45]. The nitrogen of nitro group act as an electron sink, showing a maximum electron occupancy.

### 4.4. UV-visible analysis

The time dependent density functional theory (TD-DFT) is applied to investigate the excited state properties of the molecular system. The electronic absorption spectrum of 2A3M5NP was simulated with TD-DFT with B3LYP/cc-pVTZ basis set with ethanol as solvent. The combined experimental and computed UV-Visible absorption spectra of 2A3M5NP is given in Fig. 5. The experimental spectrum shows the absorption peaks at 220 nm and 345 nm which correspond to π → π* and n → π* transitions respectively. The computed spectra show the absorption peaks appeared at 253 nm and 350 nm with an excitation energy of 4.88 eV and 3.54 eV respectively. In Table 5, the computed results of absorption spectrum are tabulated along with excited energies and oscillator strengths.

### 4.5. Frontier molecular orbital analysis

The highest occupied molecular orbital (HOMO) and lowest unoccupied molecular orbital (LUMO) are termed as the frontier molecular orbitals (FMO). The HOMO is logically viewed as nucleophilic or electron donating orbital and directly related to the ionization potential, while the LUMO is electrophilic and electron accepting orbitals related to the

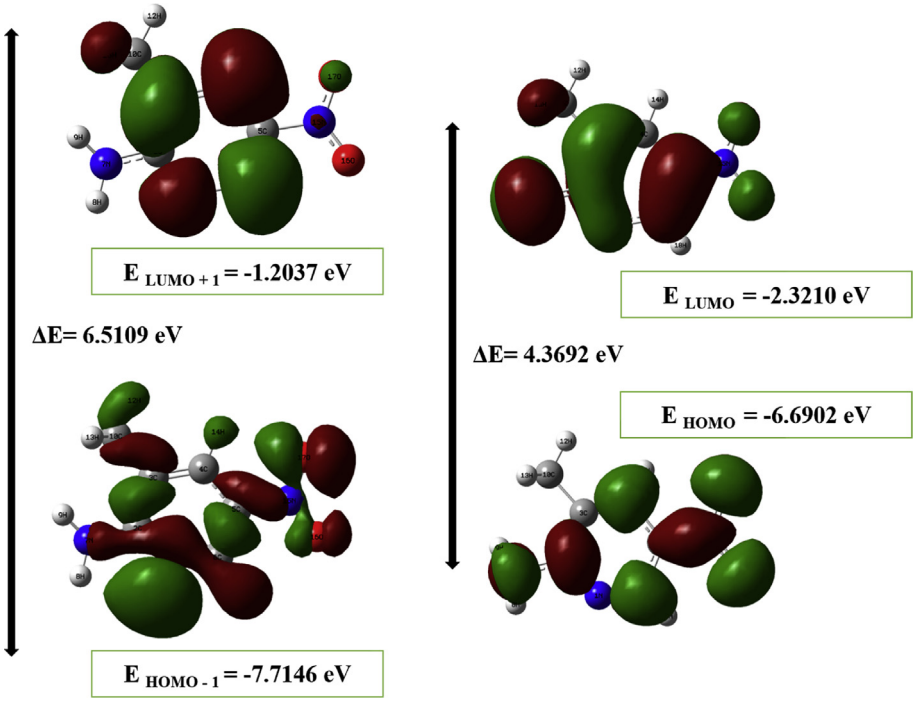


**Fig. 6.** The frontier molecular orbitals of 2A3M5NP molecule in ethanol.

**Table 6**
The chemical reactive descriptors of 2A3M5NP molecule.

| Parameters | B3LYP/cc-pVTZ (in Vacuum) |
|---|---|
| $E_{HOMO}$ (eV) | -6.6902 |
| $E_{LUMO}$ (eV) | -2.3210 |
| $E_{HOMO} - E_{LUMO}$ (eV) | 4.3692 |
| Ionization Potential [$I = -E_{HOMO}$] (eV) | 6.6902 |
| Electron affinity [$A = -E_{LUMO}$] (eV) | 2.3210 |
| Chemical hardness [$\eta = (I - A)/2$ ] (eV) | 2.1846 |
| Electronegativity [ $\mu = -(I + A)/2$ ] (eV) | -4.5056 |
| Softness [$\xi = 1/2\eta$] (eV) | 0.2288 |
| Electrophilicity index [ $\omega = \mu^2/2\eta$ ] (eV) | 4.6462 |

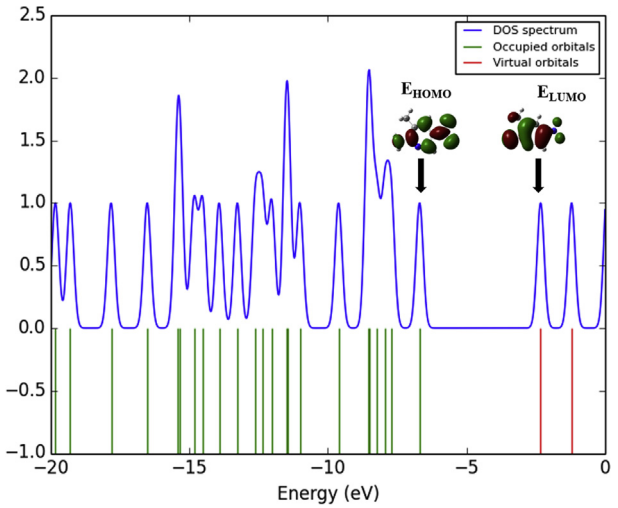


**Fig. 7.** The density of states spectrum of 2A3M5NP molecule.

electron affinity of the molecule [46, 47]. Especially for conjugated molecules, the information about the frontier molecular orbitals helps to know the charge transfer between the electron donor group and electron acceptor group through the π-conjugated path [48]. Fig. 6 depicts the HOMO and LUMO plots of 2A3M5NP molecule. The electronic transport property of the molecule is governed by the energy difference between the HOMO and LUMO orbitals. The energy gap of 2A3M5NP is found to be 4.3692 eV. In HOMO-LUMO plot, the red colour represents the positive phase of the orbital and the green colour represents the negative phase of the orbital. In HOMO, the electrons are fully localized on the entire amine group. A partial localization of electrons was seen on pyridine ring, methyl group and nitro group. The nitro group nitrogen (N15) is entirely free from electron localization. In LUMO, the localization of electrons is found on the entire nitro group. A partial localization is found on pyridine ring and amine group. The methyl group is free from the electron localization. The knowledge of the frontier molecular orbitals helps us to know about the chemical reactivity and stability of the molecule. The stability of the molecule plays an important role in bio-medically important drug designing. The difference between the $E_{HOMO}$ and $E_{LUMO}$ is termed as the energy gap of the molecule. A smaller energy gap leads to the molecule to be less stable and more reactive while large energy gap leads to more stable and less reactive system [49].

From Koopman's theorem, the chemical reactive descriptors like, ionization potential ($I = -E_{HOMO}$) = 6.6902 eV, electron affinity ($A = -E_{LUMO}$) = 2.3210 eV, chemical hardness ($\eta$) = ½ ($E_{LUMO}$-$E_{HOMO}$) = 2.1846 eV, chemical potential ($\mu$) = ½ ($E_{LUMO} + E_{HOMO}$) = -4.5056 eV, electrophilicity index ($\omega$) = ($\mu^2/2\eta$) = 4.6462 eV and electronegativity ($\chi$) = (-$\mu$) = 4.5056 eV of the molecule are evaluated by using $E_{HOMO}$ and $E_{LUMO}$ energies and are presented in Table 6. Fig. 7 shows the density of states (DOS) spectrum of the 2A3M5NP molecule. The DOS spectrum is generated using Gauss sum package [50]. The DOS spectrum provides the visual understanding of occupied molecular orbitals and unoccupied molecular orbitals of the corresponding molecule.

### 4.6. Molecular electrostatic potential analysis

The molecular electrostatic potential (MEP), V(r) is the potential energy of a test proton located at a particular distance from the molecule. The MEP analysis is used to predict the shape, size and reactivity of the molecule in 3-dimensional representation using the interaction energy between the charge distribution of the molecule and the unit positive test charge located at a distance $R_A$ [51].

$$V(r) = \sum_A \frac{Z_A}{|R_A - r|} - \int \frac{\rho(r')}{|r' - r|} dr' \quad (5)$$

where $Z_A$ represents the charge of the nucleus A located at a distance of $R_A$ and $\rho(r')$ represents the charge density at the point r'. The MEP analysis helps us to understand the molecular properties, charge density and relative polarity of the molecule in a visual way. The colour codes represent the positive and negative potential on the molecular surface. The red colour denotes the maximum negative potential region whereas the blue colour denotes the maximum positive potential region of the molecule. The colour green represents the zero potential areas of the corresponding molecule. Here, the 3D molecular electrostatic potential mapping of 2A3M5NP is presented in Fig. 8. The oxygen atoms O16 and O17 of nitro group acquire a maximum negative potential and make the site as a nucleophilic attack region. The (–M) mesomeric effect of nitro group results the region with more electronic charge leads to red in colour. On the other hand, the hydrogens H8 and H9 of amine group show the maximum positive potential region and leads to a probable electrophilic attack region with a blue colour surrounding. The delocalization of the electrons inside the pyridine ring is clearly demonstrated by

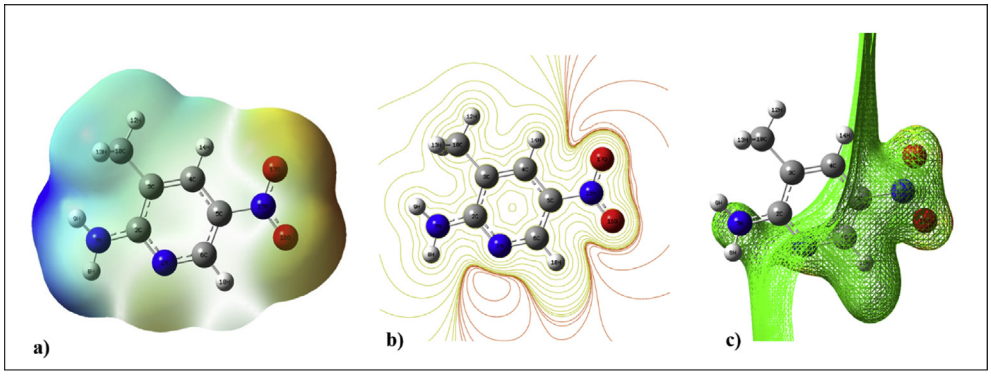


**Fig. 8.** a) The total electron density surface mapping of 2A3M5NP molecule. b) The contour mapping of 2A3M5NP molecule. c) The electrostatic potential surface of 2A3M5NP.

the greenish colour of the molecule.

## 5. Conclusion

The molecular geometry optimization of 2A3M5NP compound is carried out using DFT/B3LYP method with 6-311G (d,p), 6-311G++ (d,p) and cc-pVTZ basis sets. The optimized parameters like bond distances and bond angles of the compound are calculated. The vibrational analysis of the compound is performed for the minimum energy and the computed wavenumbers are compared with the experimental wavenumbers. The UV-Visible spectrum of the molecule is investigated and the absorption peaks are found at 220 nm and 345 nm and correspond to $\pi \rightarrow \pi^*$ and $n \rightarrow \pi^*$ transitions respectively. The NBO analysis provides the intra molecular charge transfer of the molecule. The amine group act as an electron-donor whereas the nitro group act as an electron-acceptor. The energy gap between the LUMO (Lowest Unoccupied Molecular Orbital) and HOMO (Highest Occupied Molecular Orbital) is observed as 4.3692 eV. The chemical reactive descriptors are analysed from frontier molecular orbital (FMO) analysis. The reactive sites of 2A3M5NP is analysed by molecular electrostatic potential (MEP) mapping results the oxygens O16 and O17 are nucleophilic sites. The present investigation provides the complete structural information and vibrational analysis of 2A3M5NP compound which may useful for further studies.

## Declarations

### *Author contribution statement*

Sujin P. Jose: Conceived and designed the experiments; Analyzed and interpreted the data; Contributed reagents, materials, analysis tools or data; Wrote the paper.

S. Mohan: Conceived and designed the experiments; Analyzed and interpreted the data.

S. Sivaprakash: Performed the experiments; Analyzed and interpreted the data; Wrote the paper.

S. Prakash: Analyzed and interpreted the data.

### *Funding statement*

This work was supported by a UGC-Non-NET fellowship.

### *Competing interest statement*

The authors declare no conflict of interest.

### *Additional information*

No additional information is available for this paper.

## Acknowledgements

The authors acknowledge the University Science Instrumentation Centre (USIC) of Madurai Kamaraj University (MKU) for providing FTIR spectrum. The authors would like to acknowledge the Sophisticated Analytical Instrument Facility, IITM for providing the FT-Raman spectrum.

## References

[1] Q. Tang, Y. Duan, L. Wang, M. Wang, Y. Ouyang, C. Wang, H. Mei, S. Tang, Y. Xiong, P. Zheng, P. Gong, W. Zhu, Synthesis and antiproliferative activity of pyrrolo[2,3-b]pyridine derivatives bearing the 1,8-naphthyridin-2-one moiety, Eur. J. Med. Chem. 143 (2018) 266–275.

[2] A.M. Attia, H.A. Mansour, A.A. Almehdi, M.M. Abbasi, Synthesis of some pyridine ribosides and their biological activity, Nucleosides Nucleotides 18 (1999) 2301–2306.

[3] I.O. Zhuravel, S.M. Kovalenko, A.V. Ivachtchenko, K.V. Balakin, V.V. Kazmirchuk, Synthesis and antimicrobial activity of 5-hydroxymethyl- 8-methyl-2-(N-arylimino)-pyrano[2,3-c]pyridine-3-(N-aryl)-carboxamides, Bioorg. Med. Chem. Lett 15 (2005) 5483–5487.

[4] J. Xue, J. Diao, G. Cai, L. Deng, B. Zheng, Y. Yao, Y. Song, Antimalarial and structural studies of pyridine-containing inhibitors of 1-Deoxyxylulose-5-phosphate reductoisomerase, ACS Med. Chem. Lett. 4 (2013) 278–282.

[5] L.-J. Zhang, M.-Y. Yang, Z.-H. Sun, C.-X. Tan, J.-Q. Weng, H.-K. Wu, X.-H. Liu, Synthesis and Antifungal Activity of 1,3,4-Thiadiazole Derivatives Containing Pyridine Group, (n.d.). http://www.ingentaconnect.com/content/ben/lddd/2014/00000011/00000009/art00008 (accessed June 9, 2018).

[6] F. Shi, C. Li, M. Xia, K. Miao, Y. Zhao, S. Tu, W. Zheng, G. Zhang, N. Ma, Green chemoselective synthesis of thiazolo[3,2-a]pyridine derivatives and evaluation of their antioxidant and cytotoxic activities, Bioorg. Med. Chem. Lett 19 (2009) 5565–5568.

[7] I. V Magedov, M. Manpadi, M. a Ogasawara, a S. Dhawan, S. Rogelj, S. Van Slambrouck, W.F. a Steelant, N.M. Evdokimov, P.Y. Uglinskii, E.M. Elias, Structural simplification of bioactive natural products with multicomponent synthesis. 2. Antiproliferative and antitubulin activities of pyrano [3, 2-c] pyridones and pyrano [3, 2-c] quinolones, J. Med. Chem. 51 (2008) 2561–2570.

[8] O.M. Ahmed, M.A. Mohamed, R.R. Ahmed, S.A. Ahmed, Synthesis and anti-tumor activities of some new pyridines and pyrazolo[1,5-a]pyrimidines, Eur. J. Med. Chem. 44 (2009) 3519–3523.

[9] M.L. Stems, J. a Sneha, S. Chaudhari, Alpha-amylase inhibitory and hypoglycemic activity of clerodendrone multiflorum linn. stems, Asian J. Pharmaceut. Clin Res. World Health 4 (2011) 2–5.

[10] G. Beck, K. Kesseler, E. Baader, W. Bartmann, A. Bergmann, E. Granzer, H. Jendralla, B. Von Kerekjarto, R. Krause, Synthesis and biological activity of new HMG-CoA reductase inhibitors. 1. Lactones of pyridine- and pyrimidine-substituted 3,5-dihydroxy-6-heptenoic (-heptanoic) acids, J. Med. Chem. 33 (1990) 52–60.

[11] J. Pradhan, A. Goyal, Pyridine containing azoles: possible promising antimicrobial molecules, Int. J. Pharm. Res. Allied Sci. 1 (2012) 35–42.

[12] T. Murata, M. Shimada, S. Sakakibara, T. Yoshino, H. Kadono, T. Masuda, M. Shimazaki, T. Shintani, K. Fuchikami, K. Sakai, H. Inbe, K. Takeshita, T. Niki, M. Umeda, K.B. Bacon, K.B. Ziegelbauer, T.B. Lowinger, Discovery of novel and selective IKK-beta serine-threonine protein kinase inhibitors. Part 1, Bioorg. Med. Chem. Lett 13 (2003) 913–918. http://www.ncbi.nlm.nih.gov/pubmed/12617920.

[13] B. Leal, I.F. Afonso, C.R. Rodrigues, P.A. Abreu, R. Garrett, L.C.S. Pinheiro, A.R. Azevedo, J.C. Borges, P.F. Vegi, C.C.C. Santos, F.C.A. da Silveira, L.M. Cabral, I.C.P.P. Frugulhetti, A.M.R. Bernardino, D.O. Santos, H.C. Castro, Antibacterial profile against drug-resistant Staphylococcus epidermidis clinical strain and structure-activity relationship studies of 1H-pyrazolo[3,4-b]pyridine and thieno [2,3-b]pyridine derivatives, Bioorg. Med. Chem. 16 (2008) 8196–8204.

[14] T. Zhou, D. Huang, A. Caflisch, Quantum mechanical methods for drug design, Curr. Top. Med. Chem. 10 (2010) 33–45.

[15] D. Zhou, An Introduction of Density Functional Theory and its Application, Physics, Drexel.Edu, 2007. http://www.physics.drexel.edu/~bob/Term_Reports/Zhou_Di_4.pdf.

[16] M.J. Frisch, G.W. Trucks, H.B. Schlegel, G.E. Scuseria, M.a. Robb, J.R. Cheeseman, J.a. Montgomery, T. Vreven, K.N. Kudin, J.C. Burant, J.M. Millam, S.S. Iyengar, J. Tomasi, V. Barone, B. Mennucci, M. Cossi, G. Scalmani, N. Rega, G.a. Petersson, H. Nakatsuji, M. Hada, M. Ehara, K. Toyota, R. Fukuda, J. Hasegawa, H. Ishida, T. Nakajima, Y. Honda, O. Kitao, H. Nakai, M. Klene, X. Li, J.E. Knox, H.P. Hratchian, J.B. Cross, C. Adamo, J. Jaramillo, R. Gomperts, R.E. Stratmann, O. Yazyev, A.J. Austin, R. Cammi, C. Pomelli, J. Ochterski, P.Y. Ayala, K. Morokuma, G.a. Voth, P. Salvador, J.J. Dannenberg, V.G. Zakrzewski, S. Dapprich, A.D. Daniels, M.C. Strain, O. Farkas, D.K. Malick, A.D. Rabuck, K. Raghavachari, J.B. Foresman, J.V. Ortiz, Q. Cui, A.G. Baboul, S. Clifford, J. Cioslowski, B.B. Stefanov, G. Liu, A. Liashenko, P. Piskorz, I. Komaromi, R.L. Martin, D.J. Fox, T. Keith, M.a. Al-Laham, C.Y. Peng, A. Nanayakkara, M. Challacombe, P.M.W. Gill, B. Johnson, W. Chen, M.W. Wong, C. Gonzalez, J.a. Pople, Gaussian 09W tutorial, an introd. To comput, Chem. Using G09W Avogadro Softw. (2009) 34.

[17] Dennington Roy, Todd Keith, John Millam, GaussView, Version 5, Semichem Inc., Shawnee Mission KS, 2009.

[18] M.H. Jamróz, Vibrational energy distribution analysis (VEDA): scopes and limitations, Spectrochim. Acta Part A Mol. Biomol. Spectrosc. 114 (2013) 220–230.

[19] M.A. Rajkumar, M. NizamMohideen, S.S.J. Xavier, S. Anbarasu, P.A. Devarajan, H. Stoeckli-Evans, Crystal structure of 2-amino-5-nitropyridinium sulfamate, Acta Crystallogr. Sect. E Struct. Reports Online. 71 (2015) 231–233.

[20] D. Sholl, J. Steckel, Density Functional Theory: a Practical Introduction, 2011. https://books.google.co.in/books?hl=en&lr=&id=_f994dmAdv0C&oi=fnd&pg=PT7&dq=Density+Functional+Theory,+A+Practical+Introduction,+Wiley,&ots=haED8giny5&sig=JlZ2pNsG4bpvlNrAb3HDuv0ypQE.

[21] M.W. Wong, Vibrational frequency prediction using density functional theory, Chem. Phys. Lett. 256 (1996) 391–399.

[22] A. Jellibi, I. Chaabane, K. Guidara, Vibrational spectroscopic and DFT calculation studies of a new organic–inorganic compound of bis (4-acetylanilinium) tetrachlorocadmiate (II), Phys. E Low-dimens. Syst. Nanostruct. 84 (2016) 1–9.

[23] L.J. Bellamy, The infrared spectra of complex molecules, vol. 2: advances in infrared group frequencies, Spectrochim. Acta 7 (1980) 250. http://linkinghub.elsevier.com/retrieve/pii/0371195155800343%5Cnhttps://books.google.com/books?id=doVyrgEACAAJ&pgis=1.

[24] A.S. El-Azab, Y. Sheena Mary, C. Yohannan Panicker, A.A.M. Abdel-Aziz, M.A. El-Sherbeny, C. Van Alsenoy, DFT and experimental (FT-IR and Raman) investigation of vibrational spectroscopy and molecular docking studies of 2-(4-oxo-3-phenethyl-3,4-dihydroquinazolin-2-ylthio)-N-(3,4,5-trimethoxyphenyl) acetamide, J. Mol. Struct. 1113 (2016) 133–145.

[25] G. Socrates, Infrared and Raman Characteristic Group Frequencies, 2004.
[26] R. Mohamed Asath, R. Premkumar, T. Mathavan, A. Milton Franklin Benial, Structural, spectroscopic and molecular docking studies on 2-amino-3-chloro-5-trifluoromethyl pyridine: a potential bioactive agent, Spectrochim. Acta Part A Mol. Biomol. Spectrosc. (2016).
[27] V. Arjunan, I. Saravanan, P. Ravindran, S. Mohan, Ab initio, density functional theory and structural studies of 4-amino-2-methylquinoline, Spectrochim. Acta Part A Mol. Biomol. Spectrosc. 74 (2009) 375–384.
[28] K.J.D. Silverstein, M. Robert, Webster X. Francis, Spectrometric identification of organic compounds, Org. Chem. (2005) 1–550.
[29] S. Sivaprakash, S. Prakash, S. Mohan, S.P. Jose, Molecular structure, vibrational analysis (IR and Raman) and quantum chemical investigations of 1-aminoisoquinoline, J. Mol. Struct. 1149 (2017) 835–845.
[30] N.P.G. Roeges, A Guide to the Complete Interpretation of Infrared Spectra of Organic Structures, Wiley, 1994. https://www.wiley.com/en-us/A+Guide+to+the+Complete+Interpretation+of+Infrared+Spectral+of+Organic+Structures-p-9780471939986.
[31] K. Carthigayan, V. Arjunan, R. Anitha, S. Periandy, S. Mohan, Spectroscopic and structural investigations of 4-bromomethyl-5-methyl-1,3- dioxol-2-one and 4,5-bis(bromomethyl)-1,3-dioxol-2-one by quantum chemical simulations - a comparative study, J. Mol. Struct. 1056–1057 (2014) 38–51.
[32] V. Arjunan, P. Ravindran, K. Balakrishnan, R. Santhanam, S. Mohan, Combined spectroscopic and DFT studies on 2-chloro-4-nitrotoluene and 4-chloro-2-nitrotoluene, J. Mol. Struct. 1016 (2012) 82–96.
[33] V. Arjunan, M.K. Marchewka, A. Pietraszko, M. Kalaivani, X-ray diffraction, vibrational and quantum chemical investigations of 2-methyl-4-nitroanilinium trichloroacetate trichloroacetic acid, Spectrochim. Acta Part A Mol. Biomol. Spectrosc. 97 (2012) 625–638.
[34] V. Arjunan, S. Mohan, Fourier transform infrared and FT-Raman spectra, assignment, ab initio, DFT and normal co-ordinate analysis of 2-chloro-4-methylaniline and 2-chloro-6-methylaniline, Spectrochim. Acta Part A Mol. Biomol. Spectrosc. 72 (2009) 436–444.
[35] V. Arjunan, S. Thillai Govindaraja, S. SubRamanian, S. Mohan, Conformational analysis, spectroscopic and quantum chemical investigations of 2-bromo-3-nitroacetophenone, J. Mol. Struct. 1037 (2013) 73–84.
[36] V. Arjunan, P. Ravindran, T. Rani, S. Mohan, FTIR, FT-Raman, FT-NMR, ab initio and DFT electronic structure investigation on 8-chloroquinoline and 8-nitroquinoline, J. Mol. Struct. 988 (2011) 91–101.
[37] J. Michalski, E. Kucharska, W. Sąsiadek, J. Lorenc, J. Hanuza, Intra- and inter-molecular hydrogen bonds, conformation and vibrational characteristics of hydrazo-group in 5-nitro-2-(2-phenylhydrazinyl)pyridine and its 3-, 4- or 6-methyl isomers, Spectrochim. Acta Part A Mol. Biomol. Spectrosc. 112 (2013) 263–275.
[38] E.B. Sas, M. Kurt, M. Can, N. Horzum, A. Atac, Spectroscopic studies on 9H-carbazole-9-(4-phenyl) boronic acid pinacol ester by DFT method, J. Mol. Struct. 1118 (2016) 124–138.
[39] M. Alcolea Palafox, J. Núñez, M. Gil, Accurate scaling of the vibrational spectra of aniline and several derivatives, J. Mol. Struct. Theochem. 593 (2002) 101–131.
[40] S. Gunasekaran, R.K. Natarajan, R. Rathikha, D. Syamala, Vibrational spectra and normal coordinate analysis of nalidixic acid, Indian J. Pure Appl. Phys. 43 (2005) 503–508.
[41] V. Arjunan, P.S. Balamourougane, M. Kalaivani, A. Raj, S. Mohan, Experimental and theoretical quantum chemical investigations of 8-hydroxy-5-nitroquinoline, Spectrochim. Acta Part A Mol. Biomol. Spectrosc. 96 (2012) 506–516.
[42] F. Weinhold, C.R. Landis, E.D. Glendening, What is NBO analysis and how is it useful? Int. Rev. Phys. Chem. 35 (2016) 399–440.
[43] Glendening, A. Reed, J. Carpenter, F. Weinhold, NBO Version 3.1, NBO Version 3.1. (n.d.).
[44] H. Gökce, N. Öztürk, M. Taşan, Y.B. Alpaslan, G. Alpaslan, Spectroscopic characterization and quantum chemical computations of the 5-(4-pyridyl)-1 H -1,2,4-triazole-3-thiol molecule, Spectrosc. Lett. 49 (2016) 167–179.
[45] R. Glaser, C.J. Horan, M. Lewis, H. Zollinger, σ-Dative and π-backdative phenyl cation-dinitrogen interactions and opposing sign reaction constants in dual substituent parameter relations, J. Org. Chem. 64 (1999) 902–913.
[46] Y.S. Mary, H.T. Varghese, C.Y. Panicker, M. Girisha, B.K. Sagar, H.S. Yathirajan, A.A. Al-Saadi, C. Van Alsenoy, Vibrational spectra, HOMO, LUMO, NBO, MEP analysis and molecular docking study of 2,2-diphenyl-4-(piperidin-1-yl) butanamide, Spectrochim. Acta Part A Mol. Biomol. Spectrosc. 150 (2015) 543–556.
[47] K. Fukui, Role of frontier orbitals in chemical reactions, Science (80-. ) 218 (1982) 747–754.
[48] C.H.C., M. Kertesz, Conformational Information from Vibrational Spectra of Styrene, Trans-stilbene, and Cis-Stilbene, 1997.
[49] H.G.O. Becker, Jan fleming, frontier orbitals and organic chemical reactions. 249 S., john wiley u. Sons LTD., london/New York/Syndney/Toronto 1976. Clothed £ 8,95, paperb. £ 3,95, J. Prakt. Chem. 320 (1978) 879–880.
[50] N.M. O'boyle, A.L. Tenderholt, K.M. Langner, cclib: a library for package-independent computational chemistry algorithms, J. Comput. Chem. 29 (2008) 839–845.
[51] M.J. S., S.K. D., Molecular Electrostatic Potentials: Concepts and Applications, (n.d.).